Progress In Electromagnetics Research, Vol. 166, 1–22, 2019

Retrieval Approach for Determining Surface Susceptibilities and Surface Porosities of a Symmetric Metascreen from Reflection and Transmission Coefficients

Christopher L. Holloway[1, *], Edward F. Kuester[2], and Abdulaziz H. Haddab[2]

Abstract—Recently we derived generalized sheet transition conditions (GSTCs) for electromagnetic fields at the surface of a metascreen (a metasurface with a "fishnet" structure, i.e., a periodic array of arbitrary spaced apertures in a relatively impenetrable surface). The parameters in these GSTCs are interpreted as effective surface susceptibilities and surface porosities, which themselves are related to the geometry of the apertures that constitute the metascreen. In this paper, we use these GSTCs to derive the plane-wave reflection (R) and transmission (T) coefficients of a symmetric metascreen, expressed in terms of these surface parameters. From these equations, we develop a retrieval approach for determining the uniquely defined effective surface susceptibilities and surface porosities that characterize the metascreen from measured or simulated data for the R and T coefficients. We present the retrieved surface parameters for metascreens composed of five different types of apertures (circular holes, square holes, crosses, slots, and a square aperture filled with a high-contrast dielectric). The last example exhibits interesting resonances at frequencies where no resonances exist when the aperture is not filled, which opens up the possibility of designing metasurfaces with unique filtering properties. The retrieved surface parameters are validated by comparing them to other approaches.

1. INTRODUCTION

A metasurface [1] is the surface (or two-dimensional) version of a three-dimensional metamaterial [3–9]. The simplicity and relative ease of fabrication of metasurfaces make them attractive alternatives to metamaterials [1] and [2]. We call any periodic two-dimensional structure whose thickness and periodicity are small compared to a wavelength in the surrounding media a metasurface. We can identify two important subclasses of metasurfaces, characterized by the type of topology possessed by the metasurface. Metasurfaces that have a "cermet" topology, which refers to an array of isolated (non-touching) scatterers, are called metafilms (see Fig. 1(a)), a term coined in [10]. Metasurfaces with a "fishnet" structure are called metascreens [11], see Fig. 1(b). In general, metascreens are characterized by periodically spaced apertures in an otherwise relatively impenetrable surface. There are other types of metasurfaces that exist somewhere between these two extremes; for example, a grating of arbitrarily-shaped coated parallel conducting wires is called a metagrating. Metagratings behave like a metafilm to electric fields perpendicular to the wire axes and like a metascreen for electric fields parallel to the wire axis [12]. Metafilms have been studied extensively in recent years, but although metascreens have been widely used, relatively less attention has been given to them from an electromagnetic modeling and analysis point of view.

Like that of a metamaterial, the behavior of a metasurface can be understood in terms of the electric and magnetic polarizabilities of its constituent scatterers (for a metafilm) or apertures (for a

Received 23 February 2019, Accepted 16 August 2019, Scheduled 11 October 2019
* Corresponding author: Christopher L. Holloway (christopher.holloway@nist.gov).
[1] Boulder Laboratories, U.S. Department of Commerce, National Institute of Standards and Technology (NIST), Boulder, CO 80305, USA. [2] Department of Electrical, Computer and Energy Engineering, University of Colorado, Boulder, CO 80309, USA.

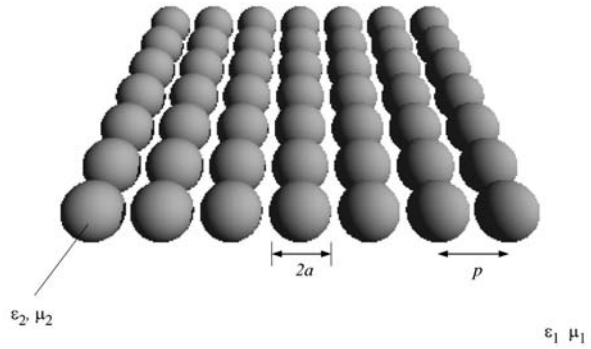

(a) metafilm: special case for an array of spherical particles

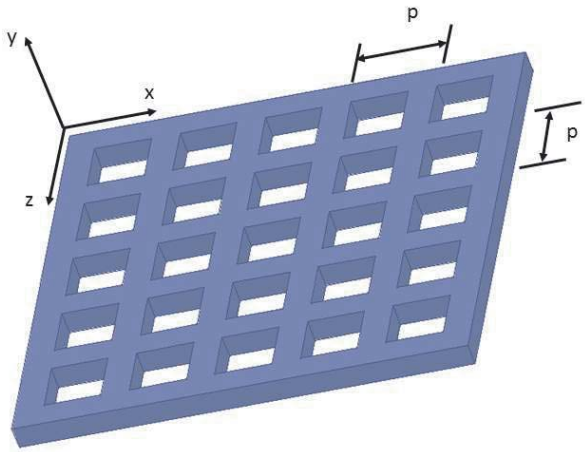

(b) metascreen: special case for an array of square apertures

Figure 1. Illustration of types of metasurfaces; (a) metafilm which consists of arbitrarily shaped scatterers placed on the xz-plane and (b) metascreen which consists of arbitrarily shaped apertures in a conducting screen located in the xz-plane.

metascreen). The traditional and most convenient method by which to model metamaterials is with effective-medium theory, using the bulk electromagnetic parameters μ_{eff} and ϵ_{eff}. Attempts to use a similar bulk-parameter model for metasurfaces have been less successful, because of ambiguities that arise [1, 13–15]. In the indicated references, it is shown that the surface susceptibilities of a metafilm are the properties that uniquely characterize a metafilm, and as such, serve as its most appropriate descriptive parameters. As a result, scattering by a metafilm is best characterized by generalized sheet-transition conditions (GSTCs) [10, 13–15] in contrast to the effective-medium description used for a metamaterial, and the coefficients appearing therein are all that are required to model the macroscopic interaction of a metafilm with an electromagnetic field. In [1], we stated (without proof) that GSTCs could also be used to model metascreens, and a detailed derivation was given recently in [11] using the method of multiple-scale homogenization. Alternatively, a dipole-interaction model can be used to obtain the GSTCs [16] and [17]. However they are obtained, the GSTCs for a metascreen take on a different form than those required for the metafilm, and their features are discussed in [11, 16] and [17]. The issue with a metascreen is that there is the possibility of having tangential surface currents (flowing on the surface of the screen along the z and x directions) that do not vanish as the lattice constant of the metascreen approaches zero; as such, a GSTC that constrains the tangential H cannot be used, see [11] for details.

The GSTCs allow the surface distribution of apertures to be replaced with a boundary condition

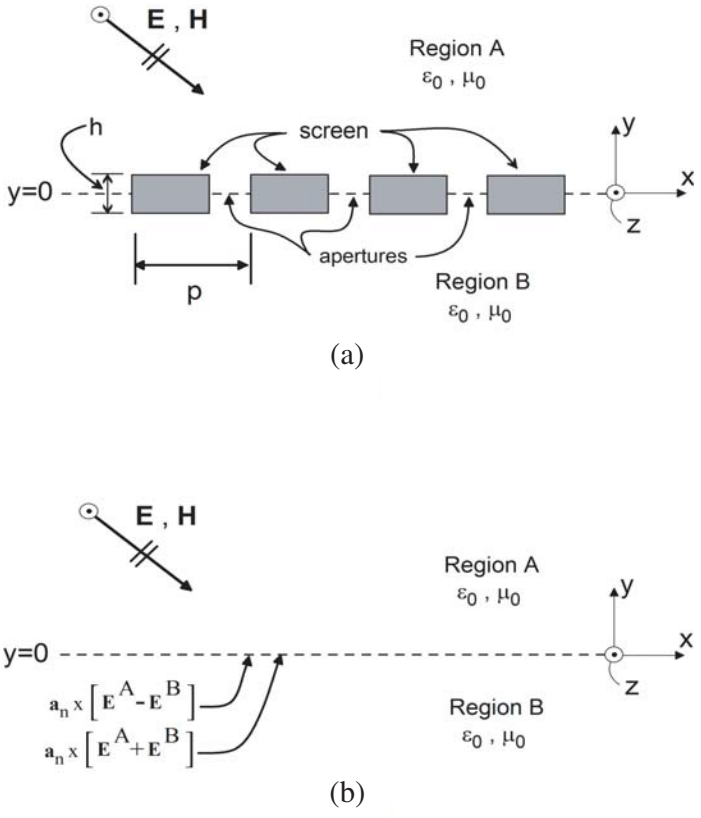

Figure 2. (a) Metascreen (array of apertures in conducting screen) and (b) the reference plane at which the GSTCs are applied.

on the averaged fields that is applied across an infinitely thin equivalent surface (hence the name metascreen), as indicated in Fig. 2. In [11], the GSTCs relating the electromagnetic fields on both sides of the metascreen shown in Fig. 1 and Fig. 2 were derived. The size, shape and spacing of the apertures as well as the material properties on both sides of the metascreen make their presence known through effective surface susceptibilities and surface porosities at the interface. It is worth noting that the GSTCs for a metafilm impose conditions on the jumps in the tangential electric and magnetic fields, which depend only on electric and magnetic effective surface susceptibilities. On the other hand, the GSTCs for a metascreen involve one condition for the jump in the tangential electric field, and another for the average of the tangential electric field, the latter of which involves surface porosities. These parameters are uniquely defined and thus represent the physical quantities that uniquely characterize the metascreen. These GSTCs, along with Maxwell's equations, are all that are needed to determine macroscopic scattering, transmission, and reflection from the metascreen.

In this paper, we use the GSTCs to derive the plane-wave reflection (R) and transmission (T) coefficients for a metascreen. The derivation presented in [11] laid out the framework for calculating the required surface susceptibilities and surface porosities, which require the solution of a set of static field problems — this can be computationally challenging for generally shaped apertures. Thus, we will also derive expressions allowing the surface parameters to be retrieved from measured or simulated values of R and T. This is analogous to the modified Nicolson-Ross-Weir (NRW) approach used for retrieving the effective permeability and permittivity of a metamaterial [18–24], and to the method used to retrieve the surface susceptibilities for a metafilm [13] and [14]. Note that the standard NRW approach for metamaterials must be modified when negative material properties exist; typically, the choice of the sign of a square-root is made unambiguous by ensuring an appropriate direction of power flow. The GSTCs given in [11] will be used here to develop retrieval techniques for a metascreen. We demonstrate this retrieval approach by showing results for metascreen composed of an array of five different types of

apertures (circular holes, square holes, crosses, slots, and a square aperture filled with a high-contrast dielectric). Finally, we discuss the behavior of the surface parameters (and discuss how to physically interpret them) at the two extreme limits of the aperture fill-factor.

It is worth noting that, while there has been a lot of work on the derivation and use of equivalent boundary conditions (EBC), notably that of Weinstein [25, 26] and of Senior and Volakis [27], only the EBCs of Sakurai [28] and of Kontorovich and his colleagues (e.g., [29]) were applicable for metascreen type structures, and these were limited to grids of the thin wire type. Only in [11] have generally applicable GSTCs for a metascreen of fairly general geometry been derived. Of the EBCs discussed in Weinstein [25], Eqs. (56.44) and (56.45) therein have the same functional form as those required for a metafilm [10, 13–15], while the other set of EBCs [(56.46) and (56.47) therein] are valid for metagrating (wire grating) type structures. However, none of these is valid for a metascreen (the structure analyzed in [11] and the present paper). Only in the particular limit of a metagrating (as discussed in Section 4.4 of this paper) does one of our surface parameters reduce to one of Weinstein's surface parameters. There are hints in the book by Senior and Volakis [27], as well as in some papers by Volakis and his colleagues [30, 31], that a "universal" GSTC might exist for an arbitrary thin metasurface, but nowhere does such a condition seem to appear explicitly, and at present we must content ourselves with the observation that topologically distinct metasurfaces (e.g., metafilms, metagratings and metascreens) have distinct GSTCs, none of which is applicable to any of the others, however similar they might appear at a superficial glance. Thus, in order to model and analyze metascreens, the GSTCs presented in this paper are required, on which the techniques for the retrieval of the surface parameters of the metascreen are based.

2. REFLECTION AND TRANSMISSION COEFFICIENTS FOR AN OBLIQUELY INCIDENT PLANE WAVE ONTO A SYMMETRIC METASCREEN

As seen from the GSTCs derived in [11] for the general case, the dyadic magnetic surface parameters may have off-diagonal terms such that coupling between transverse electric (TE) and transverse magnetic (TM) fields can occur [32]. To keep the analysis relatively simple, in this paper we will assume that the apertures are sufficiently symmetric that these off-diagonal terms are zero. We will also assume that regions A and B are both free space, and that the screen possesses mirror symmetry about the reference plane $y = 0$. These assumptions apply to many metascreens that are encountered in practice; the more general case is treated in [32].

Under these conditions, the GSTCs obtained in [11] reduce to:

$$\mathbf{a}_y \times \left[\mathbf{E}^{\mathrm{A}}(\mathbf{r}_o) - \mathbf{E}^{\mathrm{B}}(\mathbf{r}_o)\right] = -j\omega\mu_0 \left[\mathbf{a}_x \chi_{MS}^{xx} H_{x,\mathrm{av}}(\mathbf{r}_o) + \mathbf{a}_z \chi_{MS}^{zz} H_{z,\mathrm{av}}(\mathbf{r}_o)\right] - \chi_{ES}^{yy} \mathbf{a}_y \times \nabla_t E_{y,\mathrm{av}}(\mathbf{r}_o), \quad (1)$$

and

$$\begin{aligned} \mathbf{a}_y \times \mathbf{E}_{\mathrm{av}}(\mathbf{r}_o) \;=\; & -j\omega\mu_0 \left\{\mathbf{a}_x \pi_{MS}^{xx} \left[H_x^A(\mathbf{r}_o) - H_x^B(\mathbf{r}_o)\right] + \mathbf{a}_z \pi_{MS}^{zz} \left[H_z^A(\mathbf{r}_o) - H_z^B(\mathbf{r}_o)\right]\right\} \\ & -\pi_{ES}^{yy} \mathbf{a}_y \times \nabla_t \left[E_y^A(\mathbf{r}_o) - E_y^B(\mathbf{r}_o)\right]. \end{aligned} \quad (2)$$

where

$$H_{x,\mathrm{av}}(\mathbf{r}_o) = \frac{1}{2}\left[H_x^A(\mathbf{r}_o) + H_x^B(\mathbf{r}_o)\right], \quad \text{etc.} \quad (3)$$

represent the average of the fields on the two sides of the reference plane at $y = 0$. The superscripts A and B correspond to the fields in regions A and B, and $\mathbf{r}_o$ corresponds to a point in $y = 0$, see Fig. 2. In the foregoing, the surface parameters χ_{MS} and χ_{ES} are interpreted as effective magnetic and electric surface *susceptibilities* of the metascreen, while the surface parameters π_{MS} and π_{ES} are interpreted as its effective magnetic and electric surface *porosities* [11]. With respect to the general result obtained in [11], the symmetry of the apertures has resulted in:

$$\pi_{MS}^{xz} = \pi_{MS}^{zx} = \chi_{MS}^{xz} = \chi_{MS}^{zx} \equiv 0, \quad (4)$$

while the symmetry with respect to either side of the metascreen has given:

$$\begin{aligned}
\pi_{ES}^{Ayy} &= \pi_{ES}^{Byy} \equiv 2\pi_{ES}^{yy}; \quad \chi_{ES}^{Ayy} = \chi_{ES}^{Byy} \equiv \frac{1}{2}\chi_{ES}^{yy} \\
\pi_{MS}^{Axx} &= \pi_{MS}^{Bxx} \equiv 2\pi_{MS}^{xx}; \quad \chi_{MS}^{Axx} = \chi_{MS}^{Bxx} \equiv \frac{1}{2}\chi_{MS}^{xx}. \\
\pi_{MS}^{Azz} &= \pi_{MS}^{Bzz} \equiv 2\pi_{MS}^{zz}; \quad \chi_{MS}^{Azz} = \chi_{MS}^{Bzz} \equiv \frac{1}{2}\chi_{MS}^{zz}
\end{aligned} \tag{5}$$

Conditions (1)–(2) have the same form as those derived in [16] using the dipole-interaction approximation. In that paper, the reaction of the metascreen to an electromagnetic field was determined from the symmetric and asymmetric polarizabilities of a single aperture in a thick PEC screen. The derivation shows that the surface porosities are essentially the symmetric polarizabilities of the apertures per unit area on the metascreen surface, while the surface susceptibilities are essentially the asymmetric polarizabilities of the apertures per unit area on the metascreen surface.

2.1. TE Plane Wave Incident on a Metascreen

Let a metascreen be located in the plane $y = 0$ in free space. Assume that a TE polarized plane wave is incident onto the metascreen as shown in Fig. 3(a), such that the total E-field in region A ($y > 0$) is given by $\mathbf{E} = \mathbf{E}^i + \mathbf{E}^r$, where the incident and reflected fields are

$$\begin{aligned}
\mathbf{E}^i &= \mathbf{a}_z E_0 e^{-j\mathbf{k}_i \cdot \mathbf{r}} \\
\mathbf{E}^r &= \mathbf{a}_z R_{TE} E_0 e^{-j\mathbf{k}_r \cdot \mathbf{r}}.
\end{aligned} \tag{6}$$

The transmitted field in region B ($y < 0$) is given by

$$\mathbf{E}^t = \mathbf{a}_z T_{TE} E_0 e^{-j\mathbf{k}_t \cdot \mathbf{r}}, \tag{7}$$

where

$$\begin{aligned}
\mathbf{k}_t &= \mathbf{k}_i = \{\mathbf{a}_x \sin\theta - \mathbf{a}_y \cos\theta\} k_0 \\
\mathbf{k}_r &= \{\mathbf{a}_x \sin\theta + \mathbf{a}_y \cos\theta\} k_0
\end{aligned}, \tag{8}$$

$$\mathbf{r} = x\mathbf{a}_x + y\mathbf{a}_y + +z\mathbf{a}_z, \tag{9}$$

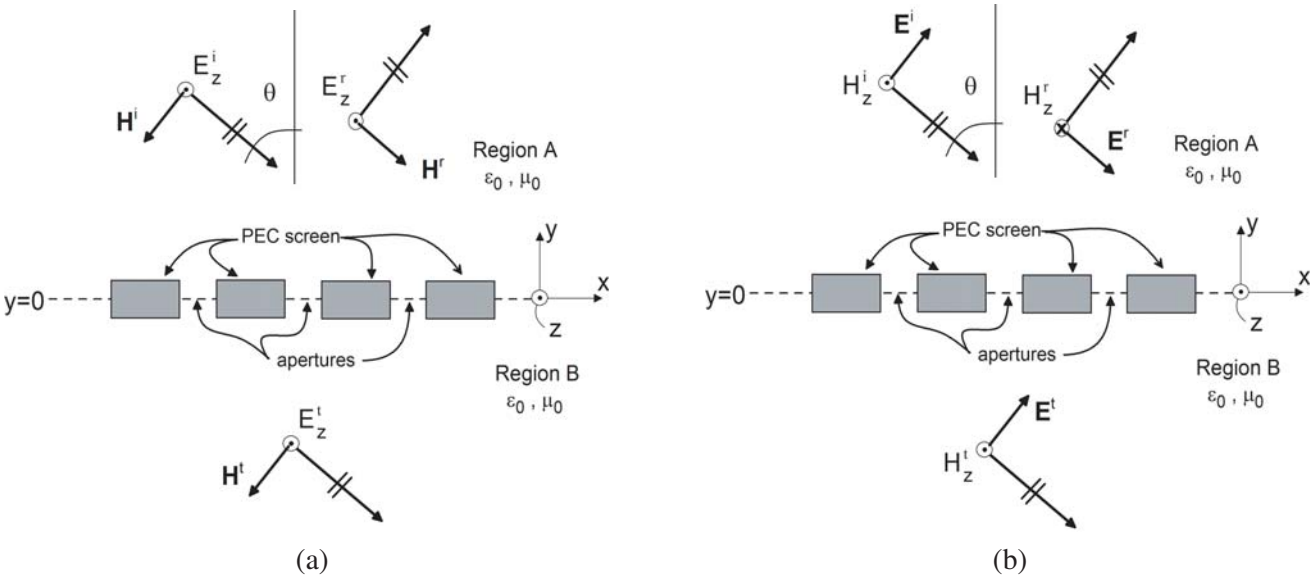

Figure 3. Plane wave incident onto a metascreen: (a) TE polarization and (b) TM polarization.

and $k_0 = \omega\sqrt{\mu_0\epsilon_0}$ is the wavenumber of free space. In Eqs. (6) and (7), R_{TE} and T_{TE} are the reflection and transmission coefficients, respectively. From Maxwell's equations, the incident, reflected and transmitted H-fields are given by:

$$\begin{aligned}
\mathbf{H}^i &= \left(\frac{k_0 E_0}{\omega\mu}\right)\{-\mathbf{a}_x\cos\theta - \mathbf{a}_y\sin\theta\}\, e^{-j\mathbf{k}_i\cdot\mathbf{r}} \\
\mathbf{H}^r &= \left(\frac{k_0 E_0 R_{TE}}{\omega\mu}\right)\{\mathbf{a}_x\cos\theta - \mathbf{a}_y\sin\theta\}\, e^{-j\mathbf{k}_r\cdot\mathbf{r}} \quad . \\
\mathbf{H}^t &= -\left(\frac{k_0 E_0 T_{TE}}{\omega\mu}\right)\{\mathbf{a}_x\cos\theta + \mathbf{a}_y\sin\theta\}\, e^{-j\mathbf{k}_t\cdot\mathbf{r}}
\end{aligned} \tag{10}$$

Substituting the electric and magnetic field components given in Eqs. (6), (7), and (10), into the GSTCs in Eqs. (1) and (2) results in

$$R_{TE}(\theta) = \frac{1 + k_0^2\,\chi_{MS}^{xx}\,\pi_{MS}^{xx}\,\cos^2\theta}{k_o^2\chi_{MS}^{xx}\,\pi_{MS}^{xx}\,\cos^2\theta - i\frac{k_0}{2}\left(\chi_{MS}^{xx} + 4\pi_{MS}^{xx}\right)\cos\theta - 1} \tag{11}$$

and

$$T_{TE}(\theta) = \frac{\frac{i\,k_o\cos\theta}{2}\left[\chi_{MS}^{xx} - 4\pi_{MS}^{xx}\right]}{k_o^2\chi_{MS}^{xx}\,\pi_{MS}^{xx}\,\cos^2\theta - i\frac{k_0}{2}\left(\chi_{MS}^{xx} + 4\pi_{MS}^{xx}\right)\cos\theta - 1} \tag{12}$$

Note that for this polarization only two surface parameters (χ_{MS}^{xx} and π_{MS}^{xx}) are needed to determine $R_{TE}(\theta)$ and $T_{TE}(\theta)$. This is in contrast to a metafilm, where three different surface parameters are needed to determine $R_{TE}(\theta)$ and $T_{TE}(\theta)$, see [1, 13, 14, 33]. The reason for this is that the two GSTCs for a metafilm are essentially duals of each other — one constraining the jump in tangential E, the other tangential H. The normal component of surface magnetic susceptibility enters into the equations in the TE case. For a metascreen, we constrain the jump and average of the tangential E field, but tangential H appears only on the right side of the GSTCs multiplied by small factors. Thus, no normal component of surface susceptibility or porosity appears, and one less parameter affects the reflection and transmission.

2.2. TM Plane Wave Incident on a Metascreen

Assume that a TM polarized H-field plane wave is incident onto the metascreen shown in Fig. 3(b), such that the H-field components of the incident, reflected, and transmitted plane waves are given by

$$\begin{aligned}
\mathbf{H}^i &= \mathbf{a}_z\frac{E_0}{\zeta_0}\, e^{-j\mathbf{k}_i\cdot\mathbf{r}} \\
\mathbf{H}^r &= -\mathbf{a}_z R_{TM}\frac{E_0}{\zeta_0}\, e^{-j\mathbf{k}_r\cdot\mathbf{r}}. \\
\mathbf{H}^t &= \mathbf{a}_z T_{TM}\frac{E_0}{\zeta_0}\, e^{-j\mathbf{k}_t\cdot\mathbf{r}}
\end{aligned} \tag{13}$$

where $\zeta_0 = \sqrt{\mu_0/\epsilon_0}$ is the wave impedance of free space. From Maxwell's equations, the incident, reflected, and transmitted E-fields are given by:

$$\begin{aligned}
\mathbf{E}^i &= E_0\left(\mathbf{a}_x\cos\theta + \mathbf{a}_y\sin\theta\right)\, e^{-j\mathbf{k}_i\cdot\mathbf{r}} \\
\mathbf{E}^r &= E_0\left(\mathbf{a}_x\cos\theta - \mathbf{a}_y\sin\theta\right) R_{TM}\, e^{-j\mathbf{k}_r\cdot\mathbf{r}}. \\
\mathbf{E}^t &= E_0\left(\mathbf{a}_x\cos\theta + \mathbf{a}_y\sin\theta\right) T_{TM}\, e^{-j\mathbf{k}_t\cdot\mathbf{r}}
\end{aligned} \tag{14}$$

Substituting these sets of expressions into the GSTCs given in Eq. (1) and (2) we obtain:

$$R_{TM}(\theta) = \frac{-\cos^2\theta - k_0^2\mathcal{A}\mathcal{B}}{\cos^2\theta - k_0^2\mathcal{A}\mathcal{B} + \frac{jk_0}{2}\cos\theta\,(\mathcal{A} + 4\mathcal{B})}, \tag{15}$$

and

$$T_{TM}(\theta) = -\frac{jk_0 \cos\theta\,[\mathcal{A} - 4\mathcal{B}]}{\cos^2\theta - k_0^2\mathcal{A}\mathcal{B} + \dfrac{jk_0}{2}\cos\theta\,(\mathcal{A} + 4\mathcal{B})}, \tag{16}$$

where

$$\begin{aligned} \mathcal{A} &= \chi_{MS}^{zz} + \chi_{ES}^{yy}\sin^2\theta \\ \mathcal{B} &= \pi_{MS}^{zz} + \pi_{ES}^{yy}\sin^2\theta \end{aligned}. \tag{17}$$

Note that for this polarization four surface parameters (χ_{MS}^{zz}, π_{MS}^{zz}, χ_{ES}^{yy}, and π_{ES}^{yy}) are needed to determine $R_{TM}(\theta)$ and $T_{TM}(\theta)$. This is in contrast to a metafilm, where only three different surface parameters are needed to determine $R_{TM}(\theta)$ and $T_{TM}(\theta)$, see [1, 13, 14, 33].

3. RETRIEVAL ALGORITHMS FOR THE SURFACE PARAMETERS

It is useful to be able to determine the surface parameters that characterize a metascreen by a method other than direct numerical computation as discussed in [11]. Such a retrieval approach for metafilms is presented in [1, 13, 14]. Here we will derive a retrieval approach applicable to metascreens.

3.1. TE Polarization

From Eqs. (11) and (12) it is seen that only two surface parameters (χ_{MSS}^{xx} and π_{MS}^{xx}) determine $R_{TE}(\theta)$ and $T_{TE}(\theta)$. Using these two expressions, the two unknown surface parameters are determined from:

$$\pi_{MS}^{xx} = \frac{j}{2k_0}\frac{R_{TE}(0) + T_{TE}(0) + 1}{R_{TE}(0) + T_{TE}(0) - 1}, \tag{18}$$

and

$$\chi_{MS}^{xx} = \frac{2j}{k_0}\frac{R_{TE}(0) - T_{TE}(0) + 1}{R_{TE}(0) - T_{TE}(0) - 1} \tag{19}$$

where $R_{TE}(0)$ and $T_{TE}(0)$ are the reflection and transmission coefficients at normal incidence ($\theta = 0^\circ$). Any angle for $R_{TE}(\theta)$ and $T_{TE}(\theta)$ in Eqs. (18) and (19) could have been used, but $\theta = 0^\circ$ is a convenient choice. If $R_{TE}(0)$ and $T_{TE}(0)$ are known, either from experimental measurements or from a numerical simulation of the metascreen, then Eqs. (18) and (19) can be used to retrieve the values of χ_{MS}^{xx} and π_{MS}^{xx}. However, if experimental data is used in these retrieval expressions, an angle other than $\theta = 0$ may be required because measuring the reflection coefficients at $\theta = 0$ can be difficult. Once these surface parameters are obtained, they can be used to determine R and T for any angle of incidence, which is demonstrated below.

3.2. TM Polarization

From Eqs. (15) and (16) we see that $R_{TM}(\theta)$ and $T_{TM}(\theta)$ depend on four of the surface parameters. Thus, unlike the TE polarization case, two sets of $R_{TM}(\theta)$ and $T_{TM}(\theta)$ data are required to determine all four unknowns for the TM polarized wave:

$$\pi_{MS}^{zz} = \frac{j}{2k_0}\frac{R_{TM}(0) + T_{TM}(0) + 1}{R_{TM}(0) + T_{TM}(0) - 1} \tag{20}$$

$$\chi_{MS}^{zz} = \frac{2j}{k_0}\frac{R_{TM}(0) - T_{TM}(0) + 1}{R_{TM}(0) - T_{TM}(0) - 1} \tag{21}$$

$$\pi_{ES}^{yy} = -\frac{\pi_{MS}^{zz}}{\sin^2\theta} + \frac{j\cos\theta}{2k_0\sin^2\theta}\frac{R_{TM}(\theta) + T_{TM}(\theta) + 1}{R_{TM}(\theta) + T_{TM}(\theta) - 1}, \tag{22}$$

and

$$\chi_{ES}^{yy} = -\frac{\chi_{MS}^{zz}}{\sin^2\theta} + \frac{2j\cos\theta}{k_0\sin^2\theta}\frac{R_{TM}(\theta) - T_{TM}(\theta) + 1}{R_{TM}(\theta) - T_{TM}(\theta) - 1} \tag{23}$$

where $R_{TM}(0)$ and $T_{TM}(0)$ are the reflection and transmission coefficients at normal incidence ($\theta = 0°$); $R_{TM}(\theta)$ and $T_{TM}(\theta)$ are the reflection and transmission coefficients at some oblique incidence angle, sufficiently different from $\theta = 0°$. With $R_{TM}(0)$, $T_{TM}(0)$, $R_{TM}(\theta)$ and $T_{TM}(\theta)$ available from either simulation or experiment, Eqs. (20)–(23) can be used to retrieve the four unknown surface parameters (χ_{MS}^{zz}, π_{MS}^{zz}, χ_{ES}^{yy}, and π_{ES}^{yy}). Here again, once these surface parameters are obtained, they can be used to determine R and T for any angle of incidence.

In the retrieval approaches for both polarizations, it is important to realize that the reference plane for $R_{TE,TM}(0)$, $T_{TE,TM}(0)$, $R_{TM}(\theta)$, and $T_{TM}(\theta)$ is required to be located at $y = 0$. This is a consequence of how the GSTCs were derived in [11]. The GSTCs (and the surface parameters) would need to be modified for different choices of reference plane location [26, 27, 34].

It is interesting to observe that the expressions for three of the retrieved surface susceptibilities for a metascreen [χ_{MS}^{xx}, χ_{MS}^{zz}, and χ_{ES}^{yy}, see Eqs. (19), (21), and (23] are the same expressions as those for three of the surface parameters for a metafilm (see Eqs. (10) and (11) in [14]). There is no reason *a priori* to think that this should be the case, and we have only been able to prove this by going through the analysis presented in this paper. The underlying reason for this is most likely that both the metascreen and metafilm have as one of their GSTCs a condition of the same form for the jump in the E-field. We emphasize that a metascreen (treated in this paper) is a very different structure than a metafilm, which was addressed in [14]). However, the second of the GSTCs the metascreen requires a set of conditions on the "average" E-fields, while the metafilm has a condition on the "jump" in the H-field (the metagrating has GSTCs that are a sort of hybrid of these two conditions). It is worth emphasizing again that the GSTCs required for a metascreen cannot be reduced to those required for a metafilm simply by taking some kind of limit or special case.

Although in this paper we have considered only the case of a PEC screen, a similar but more involved derivation can be carried out to derive GSTCs and retrieval algorithms for the case of a screen that is merely a good conductor. This requires the use of "stiff" homogenization techniques, such as those used in [35–39]. It can be shown that the final desired GSTCs will have the same functional form as for the PEC screen, and the retrieval algorithms will have similar forms to those given above. If the screen is not highly conducting (as will be the case for metals at optical frequencies), GSTCs of a rather more complicated form are to be expected — this question is beyond the scope of this paper and will be the topic of a future publication.

4. RETRIEVED SURFACE PARAMETERS FOR FIVE TYPES OF APERTURE ARRAYS

In order to illustrate the validity of these expressions for retrieving the surface susceptibilities and porosities of a metascreen, we will consider five examples.

4.1. Metascreen Composed of an Array of Circular Apertures

We first consider an array of circular apertures in a perfect conductor of thickness h as shown in Fig. 4(a). For this metascreen, $p = 100\,\text{mm}$, and a is the radius of the apertures (which will be varied). We show results for three different h ($h = 10\,\text{mm}$, $h = 5\,\text{mm}$, and $h = 0.1\,\text{mm}$). The reflection and transmission coefficients for the metascreen were determined numerically from the finite-element software HFSS (mentioning this product does not imply an endorsement, but serves to clarify the numerical program used) for both $\theta = 0°$ and $\theta = 30°$ at a frequency of 500 MHz and a/p ranging from 0 to 0.5. The numerical values for $R_{TM}(0)$, $T_{TM}(0)$, $R_{TM}(\theta)$ and $T_{TM}(\theta)$ at the reference plane $y = 0$ for $h = 5\,\text{mm}$ are shown in Fig. 5, and were used in (20)–(23) to determine the four unknown surface parameters (χ_{MS}^{zz}, π_{MS}^{zz}, χ_{ES}^{yy}, and π_{ES}^{yy}). Note that since the apertures in the array are symmetric, we have $\pi_{MS}^{xx} = \pi_{MS}^{zz}$ and $\chi_{MS}^{xx} = \chi_{MS}^{zz}$.

Figures 6 and 7 show the retrieved magnetic and electrical surface parameters for $h = 10\,\text{mm}$, $h = 5\,\text{mm}$, and $h = 0.1\,\text{mm}$. Using dipole-interaction approximations, closed-form results for these surface porosities and susceptibilities have been obtained in [16] for an array of circular apertures (Eqs. (21), (23), (30), (59)–(62) therein). These approximations are also shown in Figs. 6 and 7. From the comparison in these two figures, we see that the retrieved surface electric and magnetic susceptibility

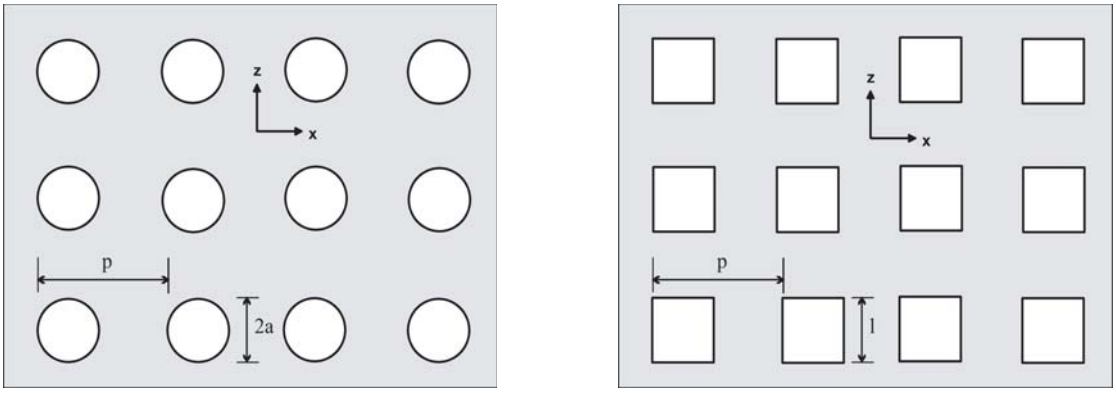

(a) array of circular apertures (b) array for square apertures

Figure 4. Metascreen composed of (a) circular apertures and (b) square apertures.

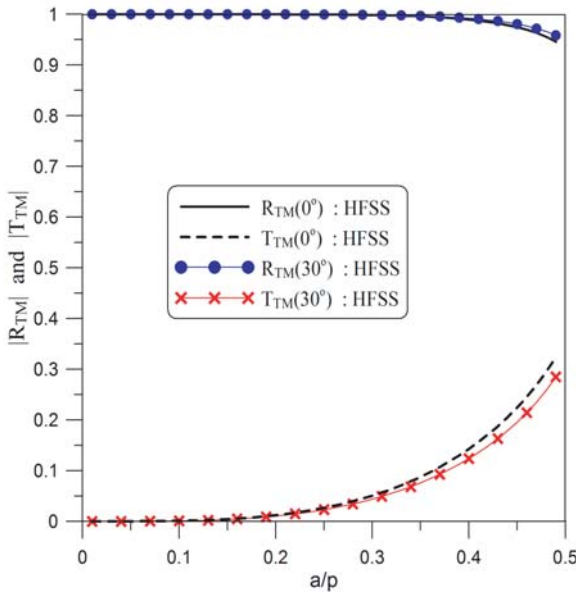

Figure 5. Numerical values for $|R_{TM}|$ and $|T_{TM}|$ for a metascreen composed of circular apertures with $p = 100\,\text{mm}$, $h = 5\,\text{mm}$, and frequency of 500 MHz.

and surface magnetic porosity correlate very well with the dipole-interaction approximation for the whole range of $a/p = 0$ to $a/p = 0.49$. While it is expected that the dipole-interaction approximation may not be valid for closely packed apertures (large a/p), it is interesting that good correlation is observed over the entire a/p range for the array of circular apertures. The surface parameters can also be determined from a static field solution obtained from an homogenization approach [11]. For further verification that the retrieval approach is valid, we compare to the homogenization approach given in [11], see Fig. 8.

4.2. Metascreen Composed of an Array of Square Apertures

Next, we consider an array of square apertures in a perfectly conducting plate as shown in Fig. 4(b). For this array, $p = 100\,\text{mm}$ and l is the length of the side of the square (which will be varied). The reflection and transmission coefficients for the metascreen were again determined numerically with HFSS for both $\theta = 0^\circ$ and $\theta = 30^\circ$ at 500 MHz and for l/p ranging from 0 to 1.0. The numerical values for $R_{TM}(0)$, $T_{TM}(0)$, $R_{TM}(\theta)$ and $T_{TM}(\theta)$ at the reference plane $y = 0$ are shown in Fig. 9 for $h = 5\,\text{mm}$, and were

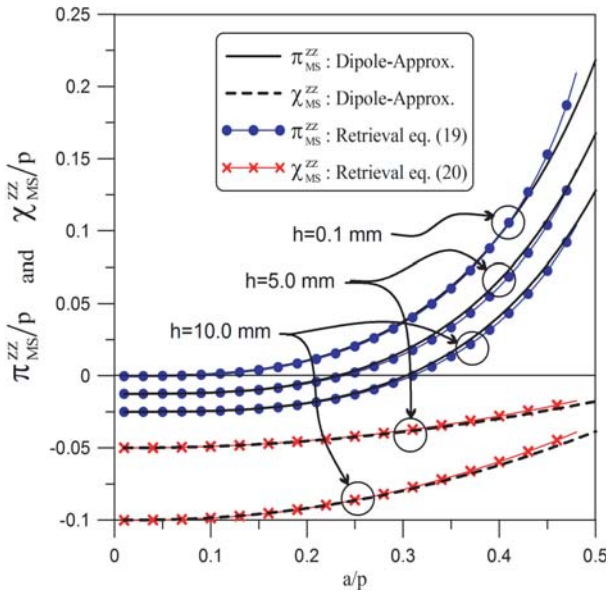

Figure 6. Magnetic surface susceptibility and surface porosity for an array of circular apertures: $p = 100\,\text{mm}$ and for $h = 10\,\text{mm}$, $h = 5\,\text{mm}$, and $h = 0.1\,\text{mm}$.

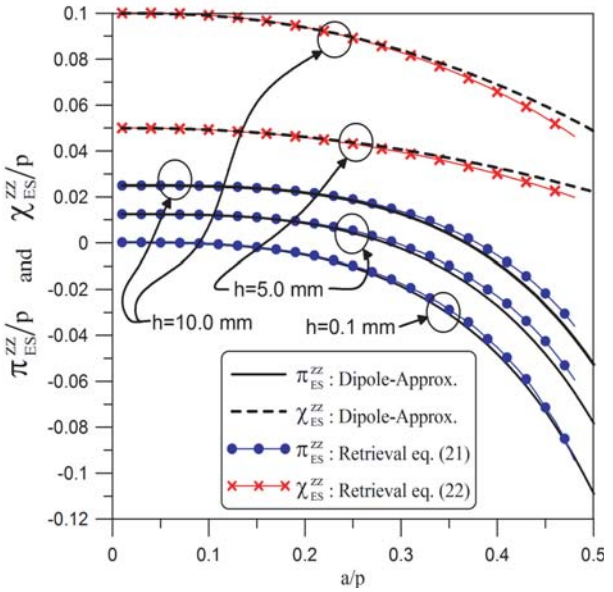

Figure 7. Electric surface susceptibility and surface porosity for an array of circular apertures: $p = 100\,\text{mm}$ and for $h = 10\,\text{mm}$, $h = 5\,\text{mm}$, and $h = 0.1\,\text{mm}$.

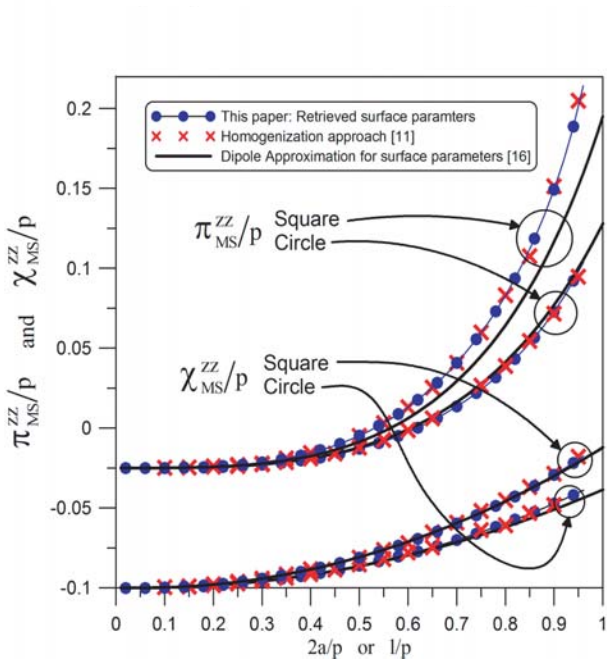

Figure 8. Comparison of the retrieved surface parameters to those obtained from the homogenization approach and to the dipole-approximations.

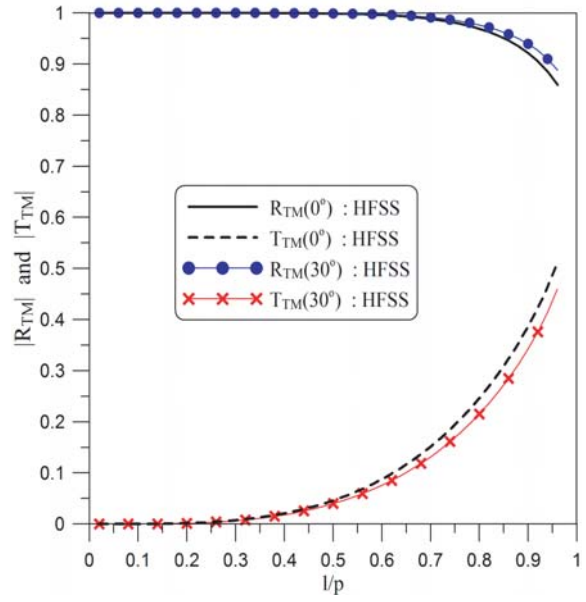

Figure 9. Numerical values for $|R_{TM}|$ and $|T_{TM}|$ for a metascreen composed of square apertures with $p = 100\,\text{mm}$, $h = 5\,\text{mm}$, and frequency of 500 MHz.

used in Eqs. (20)–(23) to determine the four unknown surface parameters (χ_{MS}^{zz}, π_{MS}^{zz}, χ_{ES}^{yy}, and π_{ES}^{yy}). Here again, since the apertures in the array are symmetric, $\pi_{MS}^{xx} = \pi_{MS}^{zz}$ and $\chi_{MS}^{xx} = \chi_{MS}^{zz}$. Figs. 10 and 11 show the retrieved magnetic and electrical surface parameters for $h = 0.1\,\text{mm}$, $h = 5\,\text{mm}$ and $h = 10\,\text{mm}$. Approximate closed-form expressions for these surface parameters for an array of square apertures are given in [16] (Eqs. (21), (23), (30), (63)–(66) therein). These dipole-approximations are also shown in Figs. 10 and 11. From this comparison, the retrieved values for the surface parameters

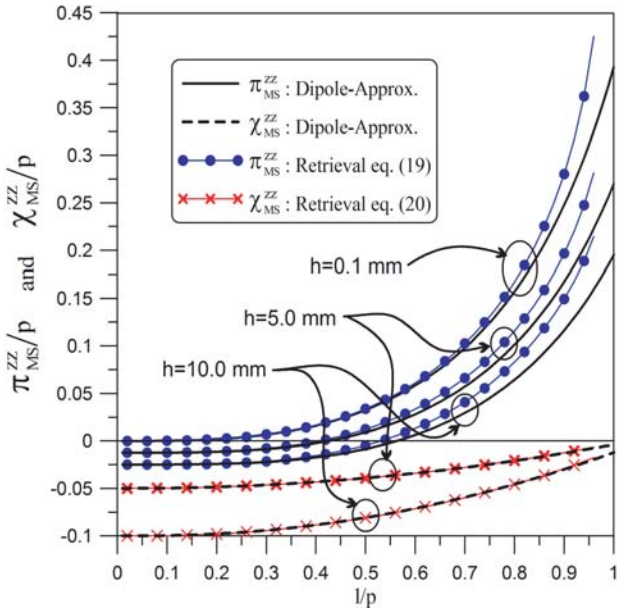

Figure 10. Magnetic surface susceptibility and surface porosity for an array of square apertures: $p = 100\,\text{mm}$ and for $h = 10\,\text{mm}$, $h = 5\,\text{mm}$, and $h = 0.1\,\text{mm}$.

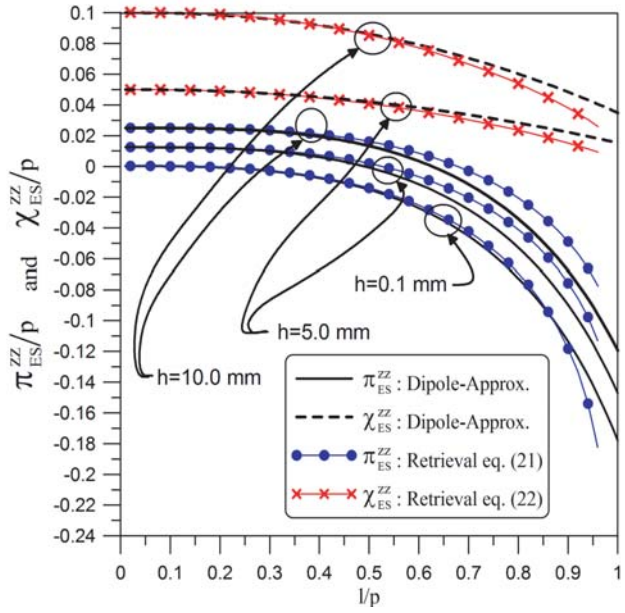

Figure 11. Electric surface susceptibility and surface porosity for an array of square apertures: $p = 100\,\text{mm}$ and for $h = 10\,\text{mm}$, $h = 5\,\text{mm}$, and $h = 0.1\,\text{mm}$.

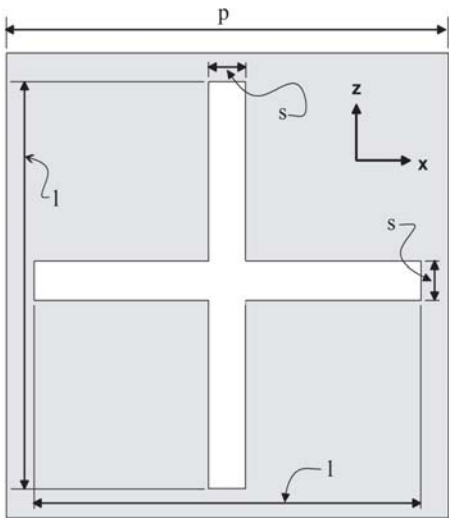

(a)

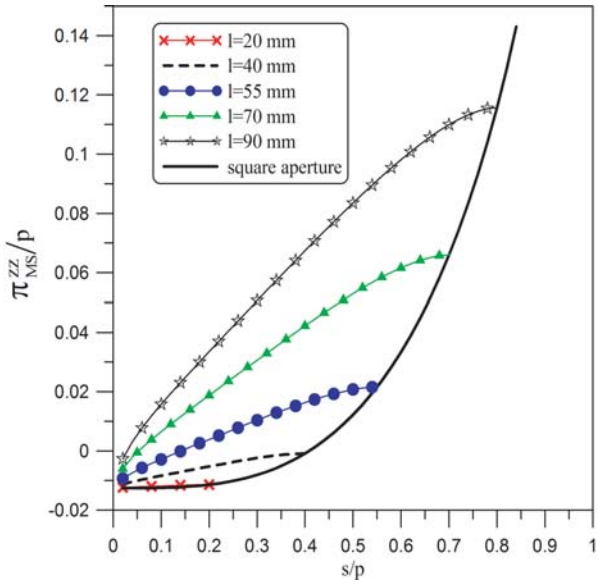

(b)

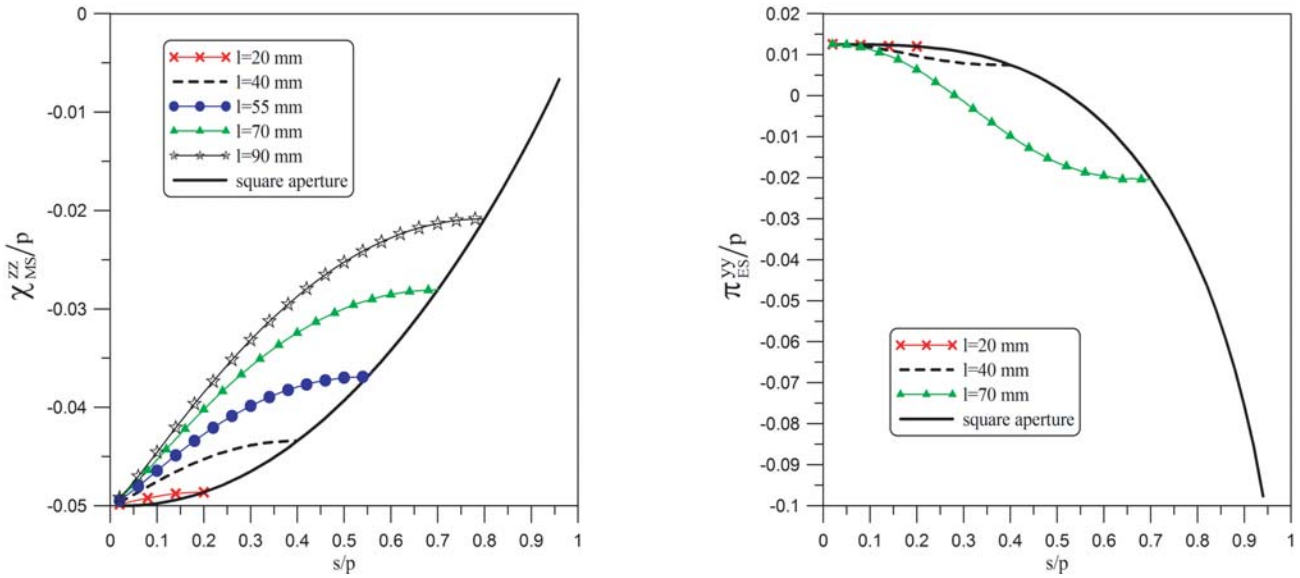

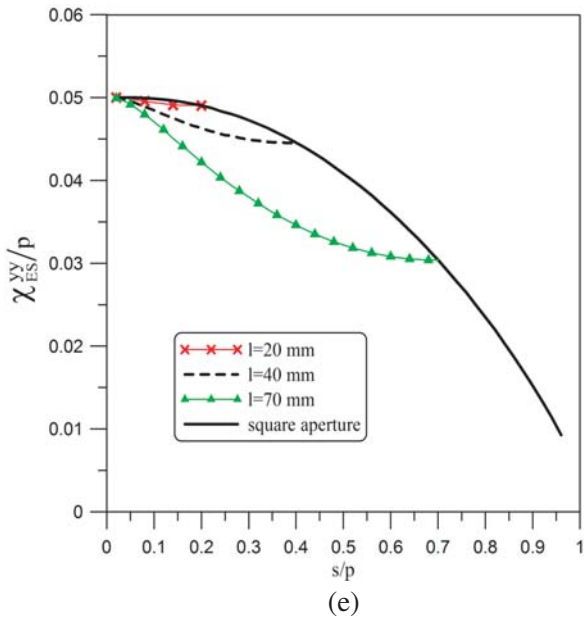

Figure 12. Retrieved surface parameters for an array of cross-shaped apertures as a function of s/l for a thickness $h = 5\,\text{mm}$ and $p = 100\,\text{mm}$: (a) periodic cell of the slot, (b) π^{zz}_{MS}, (c) χ^{zz}_{MS}, (d) π^{yy}_{ES}, and (e) χ^{yy}_{ES}.

correlated very well to those from the dipole-approximation for $l/p < 0.7$. As discussed below, as $l/p \to 1$, π_{ES} and π_{MS} should approach ∞. While the retrieved values approach this limit, we see that the dipole-model does not approach this limit. The discrepancy in the dipole-model is most likely due to the fact that some of parameters used in the dipole-approximation for the square aperture give in [16] are known to be in error by as much as 20% [16]. For further verification that the retrieval approach is valid, we compare to the homogenization approach given in [11], see Fig. 8. This comparison illustrates some of the limitations in the dipole-approximations and indicate that the surface parameters are better determined either from the homogenization-based approach or from the retrieval approach.

4.3. Metascreen Composed of an Array of Cross-Shaped Apertures

In this example we consider a metascreen composed of the cross-shaped apertures shown in Fig. 12(a). Here we show results for the surface parameters for various values of the slot length (l) and the slot width (s). In doing such, we consider the following two cases, (1) we set the length of the crosses to a constant and vary the slot width, and (2) we set the width of the crosses to a constant and vary the slot length. In all these cases the thickness of the apertures is 5 mm. Using HFSS we calculate the the $R(\theta)$ and $T(\theta)$ for both 0° and 30° incident angles for both the TE and TM polarizations. The reflection and transmission coefficient were used in Eqs. (20)–(23) to obtain the surface parameters. Figs. 12(b)–12(e) show results for the surface parameters as a function s for different values for l. Note that $\pi^{xx}_{MS} = \pi^{zz}_{MS}$ and $\chi^{xx}_{MS} = \chi^{zz}_{MS}$. Once $s = l$, the aperture reduces to a square aperture, therefore, for a reference, we

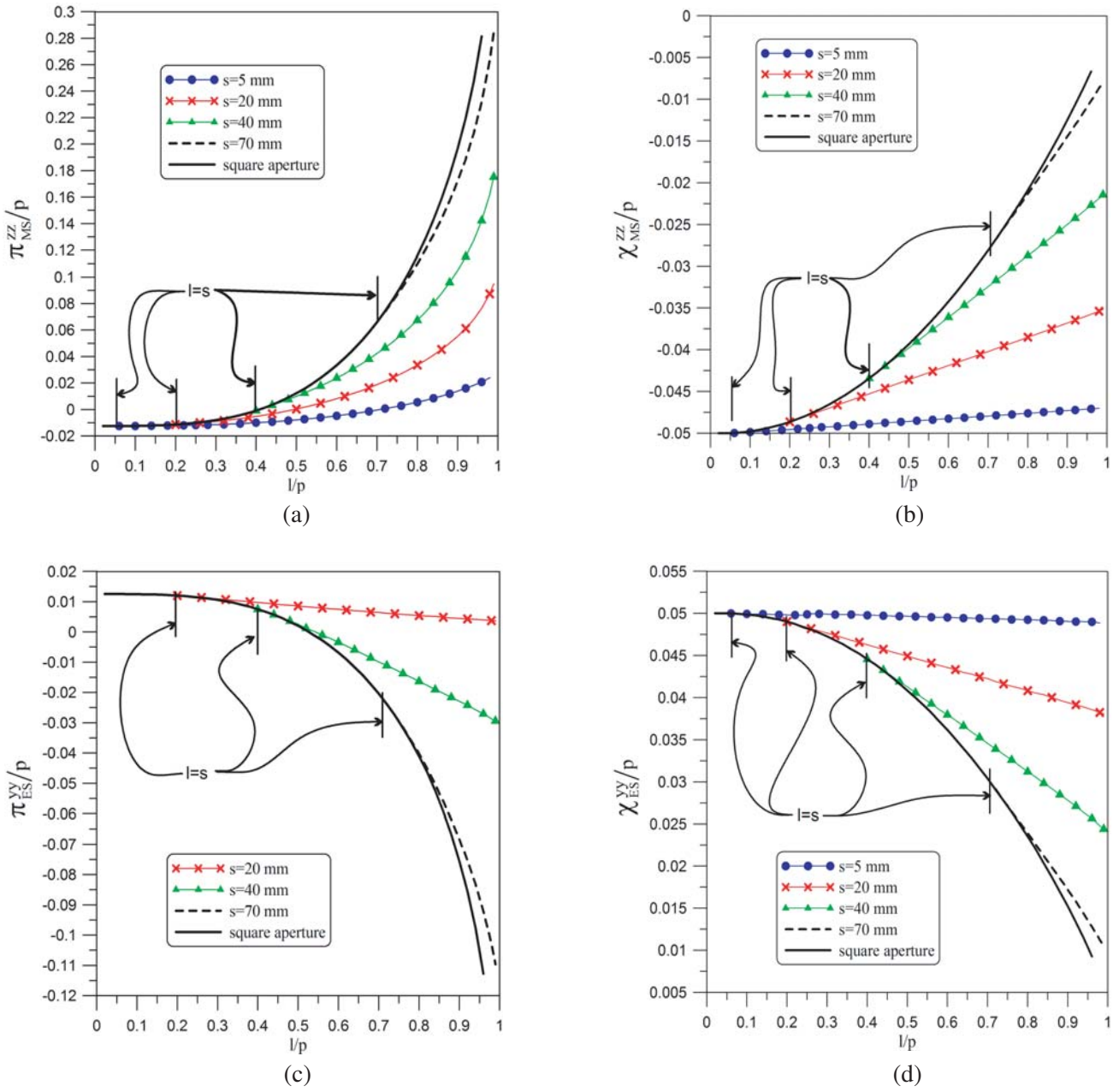

Figure 13. Retrieved surface parameters for an array of cross-shaped apertures as a function of l/p for a thickness $h = 5$ mm and $p = 100$ mm: (a) π^{zz}_{MS}, (c) χ^{zz}_{MS}, (c) π^{yy}_{ES}, and (d) χ^{yy}_{ES}.

also show the results of the square aperture. Figs. 13(a)–13(d) show results for the surface parameters as a function of l for different values of s. Again, when $l = s$, the aperture reduces to a square aperture, therefore, for a reference, we also show the results of the square aperture.

It is interesting to observe that when $l/p = 1$, the metascreen converts to a metafilm (i.e., the array of crosses converts to an array of square plates). When this occurs, one must use the GSTCs for a metafilm [1, 10, 13–15] to analyze the metasurface.

4.4. Metascreen Composed of an Array of Slot Apertures

Next, we consider a metascreen composed of the slot apertures shown in Fig. 14. Here we show results for the surface parameters for various values of the slot length (l) and the slot width (s). In all these cases the length of the slot (l) is along the x-axis and the thickness of the apertures is 0.1 mm. In the limit as $l/p \to 1$ this structure reduces to an array of metallic strips, which will allow us to make comparisons to analytical values for π^{xx}_{MS} as both $l/p \to 1$ and as $h \to 0$. The HFSS calculated reflection and transmission coefficients for this structure were used in Eqs. (18)–(23) to obtained the

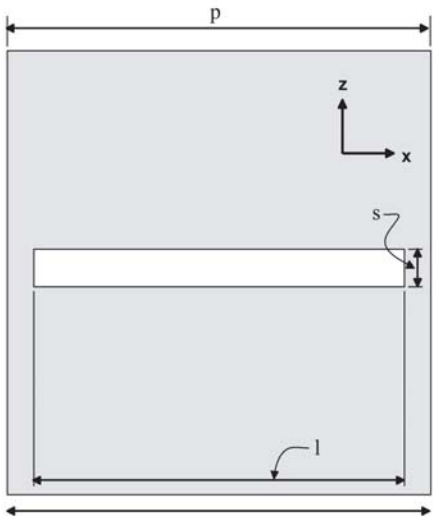

(a)

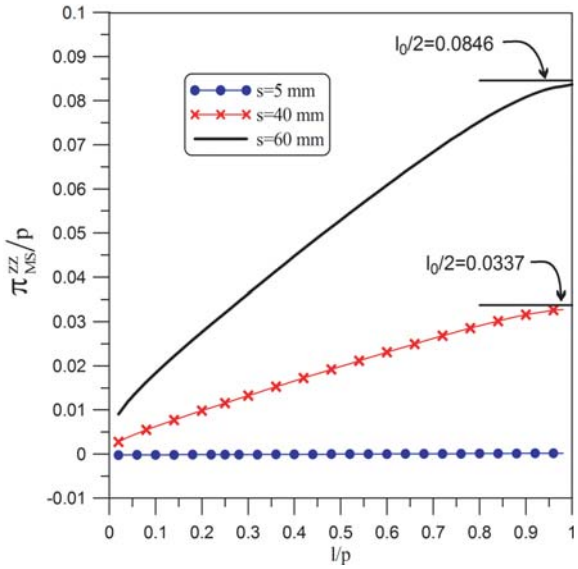

(b)

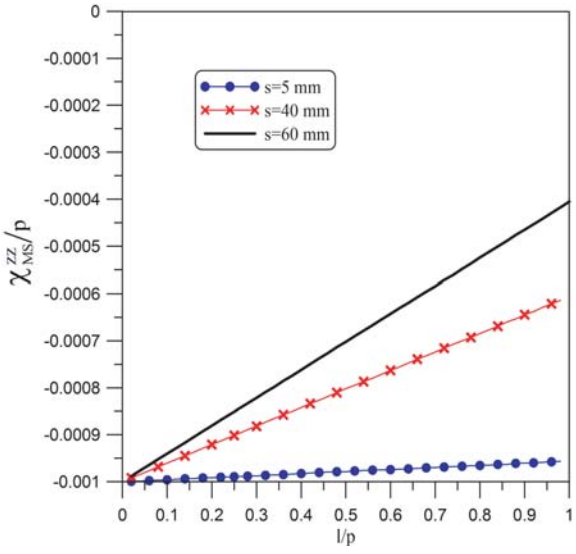

(c)

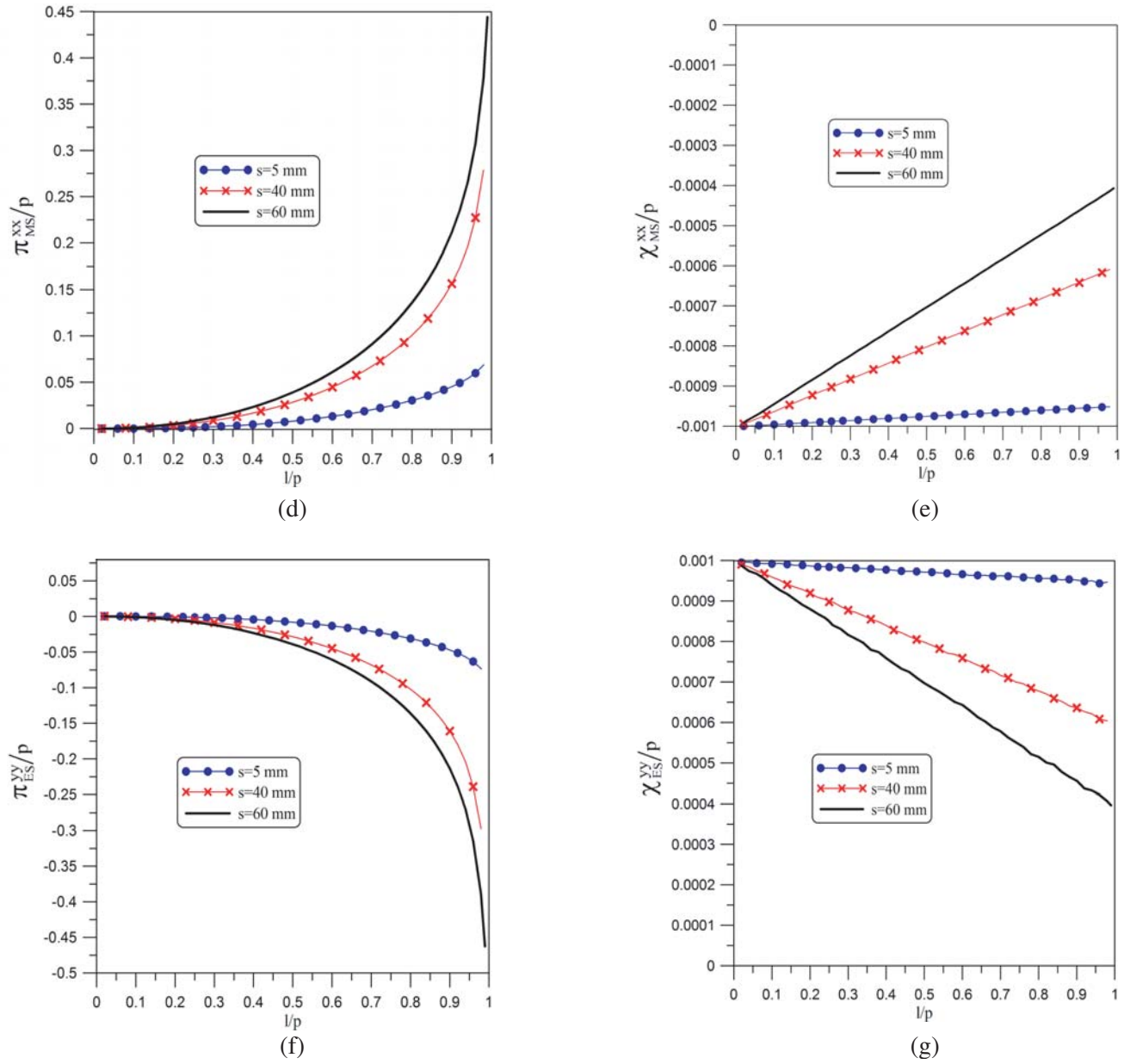

Figure 14. Retrieved surface parameters for an array of slots as a function of l/p for a thickness $h = 0.1$ mm: (a) period cell, (b) π^{zz}_{MS}, (c) χ^{zz}_{MS}, (d) π^{xx}_{MS}, (e) χ^{xx}_{MS}, (f) π^{yy}_{ES}, and (g) χ^{yy}_{ES}.

surface parameters. Figs. 14(b)–14(g) show results for the surface parameters as a function of l for different s. Note that $\pi^{xx}_{MS} \neq \pi^{zz}_{MS}$ and $\chi^{xx}_{MS} \neq \chi^{zz}_{MS}$ for this structure. As $l/p \to 1$ this structure reduces to the flat metal strip grating analyzed in [26]. In [26] Weinstein used five surface parameters in his boundary conditions and labeled them as l_0, l_1, l_2, l_3, and l_4 and obtained approximate analytical expressions for them when the strip is infinitely thin. Weinstein's parameter $l_0/2$ (see Eq. (2.96) in [26]) is equivalent to our π^{zz}_{MS} when $l/p \to 1$ in our slot case (or more precisely $\pi^{zz}_{MS} \to l_0/2$ as $l/p \to 1$ and $h \to 0$). In Fig. 14(b) we also show $l_0/2$, and we see that π^{zz}_{MS} approaches $l_0/2$ as $l/p \to 1$. Also, for a thin strip grating $\chi^{zz}_{MS} \to l_2$ $\chi^{xx}_{MS} \to l_3$, and $\chi^{yy}_{ES} \to l_4$ as $l/p \to 1$ and $h \to 0$, Weinstein shows that $l_2 = l_3 = l_4 \equiv 0$ when $h = 0$. From Fig. 14, we also see that the surface parameters χ^{xx}_{MS}, χ^{xx}_{MS}, and χ^{yy}_{ES} are very small and all approach zero as $l/p \to 1$ and $h \to 0$ (i.e., the thin slot array approaches a strip grating).

4.5. Metascreen Composed of an Array of Square Apertures Filled with a High-Contrast Dielectric

In the last example, we consider a metascreen composed of an array of square apertures filled with a dielectric with $\epsilon_r = 108.2$ and a loss tangent of $\tan\delta = 4.9 \times 10^{-5}$ (these material properties represent a commercially available material). This example illustrates three important points. First we show that the retrieval approach can also be used on a metascreen composed of lossy materials such that $\chi_{(ES,MS)}$ and $\pi_{(ES,MS)}$ have both "real" and "imaginary" parts. Secondly, we illustrate that the retrieved surface parameters can be used to determine the transmission (or reflection) coefficient for any arbitrary angle of incidence. Thirdly, we show that by filling the apertures with a high-contrast magneto-dielectric material (material with high-contrast electric and/or magnetic properties), it is possible to obtain interesting resonances at frequencies where no resonances exist when the aperture is not filled. Such behavior is not unexpected (after all, the apertures are filled with what are essentially dielectric resonators). Nevertheless, the retrieval technique developed in the present paper can obtain values for the surface susceptibilities and porosities, which in turn can be used to predict the behavior of a resonant metascreen under more general conditions (e.g., off-axis reflection and transmission coefficients, as shown below). This can lead to the possibility of designing metascreens with unique transmission and reflection properties (e.g., narrow-band filters as well as other applications).

Figure 15 shows the normal-incidence transmission coefficient as a function of frequency for an array of square apertures filled with a dielectric material ($\epsilon_r = 108.2$ and $\tan\delta = 4.9 \times 10^{-5}$). These results were obtained with HFSS for $p = 26\,\text{mm}$, $h = 10\,\text{mm}$, and $l = 10\,\text{mm}$, see Fig. 4(b). In Fig. 15, we also show results for the case when no material is in the apertures. Comparing the two results in this figure, we see that the presence of the material filling the aperture caused two resonances (at 1.63 GHz and 2.33 GHz) which are not present when no material is used. We see that at 1.63 GHz and 2.33 GHz, the surface allows almost 100% transmission (the losses cause this to be $< 100\%$) over two narrow frequency bands. These two high-transmission regions are a result of internal resonances in the high-contrast material filling the apertures.

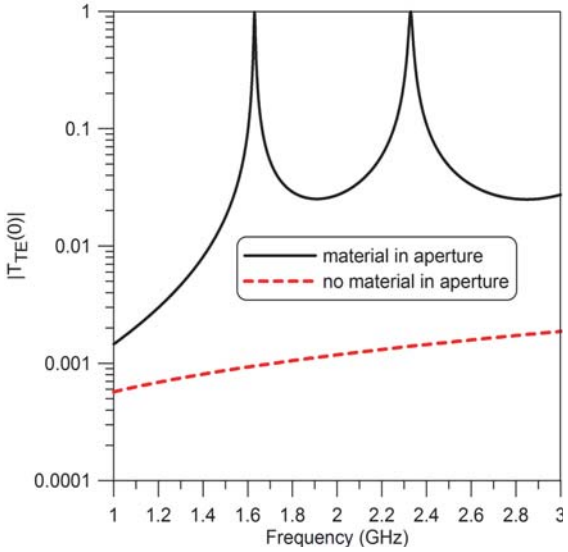

Figure 15. HFSS results for the transmission coefficient for an array of square apertures: $p = 26\,\text{mm}$, $h = 10\,\text{mm}$, and $l = 10\,\text{mm}$.

By retrieving the various surface parameters, we can get an indication as to which of the surface parameters give rise to the resonances in the transmission coefficient. Using the HFSS results for $R_{TE}(0)$ and $T_{TE}(0)$ for this metascreen, we used Eqs. (18) and (19) to determine π_{MS}^{xx} and χ_{MS}^{xx}. These retrieved values are shown in Fig. 16. Shown here are the real and imaginary parts of the surface parameters (where the imaginary parts arise due to the loss tangent of the material). Note that in these figures we have only shown results zoomed in around the two resonant frequencies. From the figure, we see

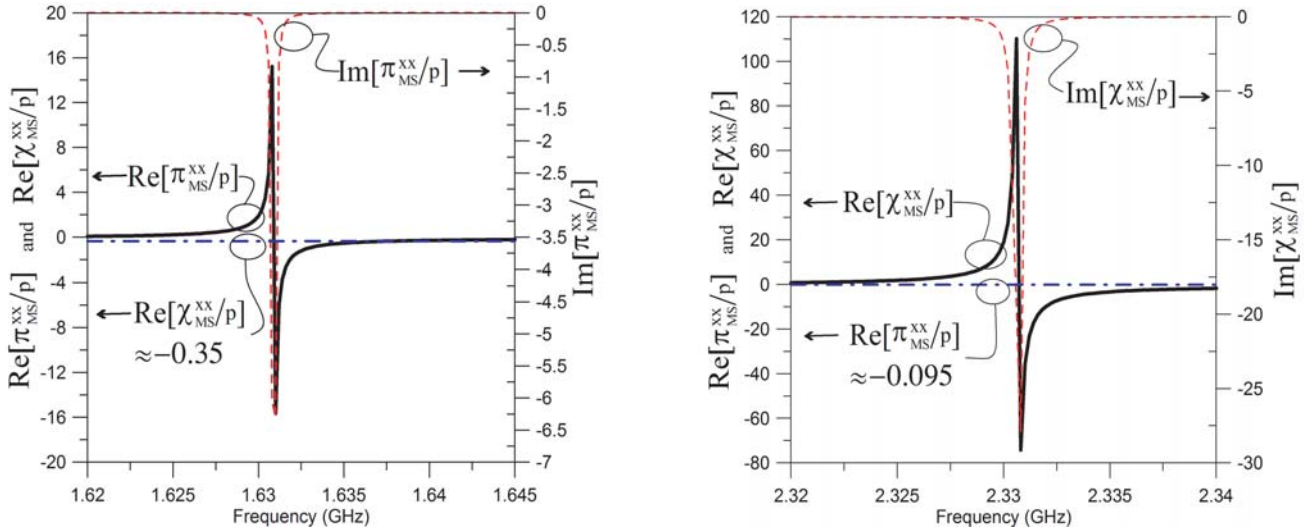

Figure 16. Retrieved surface parameters (π_{MS}^{xx} and χ_{MS}^{xx}) for an array of square aperture filled with a high-contrast material ($\epsilon_r = 108.2$ and $\tan\delta = 4.9 \times 10^{-5}$) for $p = 26\,\text{mm}$, $h = 10\,\text{mm}$, and $l = 10\,\text{mm}$: (a) 1.63 GHz and (c) 2.33 GHz.

that π_{MS}^{xx} exhibits a resonance at 1.63 GHz, while χ_{MS}^{xx} has a flat response (and is about two orders of magnitude smaller) in this same frequency range. The resonance in π_{MS}^{xx} is what gives rise to the enhanced transmission at 1.63 GHz. On the other hand, χ_{MS}^{xx} exhibits a resonance at 2.33 GHz (π_{MS}^{xx} does not and is about three orders of magnitude smaller) and χ_{MS}^{xx} is what gives rise to the enhanced transmission at 2.33 GHz.

Using these retrieved values for π_{MS}^{xx} and χ_{MS}^{xx}, along with Eq. (12), the transmission coefficient for various angles of incidence can be determined (recall that only two surface parameters are needed to determine the transmission coefficient for a TE wave). The values for $T_{TE}(\theta)$ calculated from Eq. (12) and the results given in Fig. 16 are shown in Fig. 17 for 30°, 45°, and 60°. For a comparison, also in this figure, we show numerical results obtained from HFSS. These comparisons show that the transmission coefficient obtained from surface parameters retrieved from normal incidence data are indistinguishable from the HFSS results, even for angles as high as 60°.

As shown in Eq. (16), $T_{TM}(\theta)$ for an arbitrary angle of incidence requires four surface parameters (π_{MS}^{zz}, χ_{MS}^{zz}, π_{ES}^{yy}, and χ_{ES}^{yy}). Since this metascreen is symmetric, $\pi_{MS}^{zz} = \pi_{MS}^{xx}$ and $\chi_{MS}^{zz} = \chi_{MS}^{xx}$ (which are given in Fig. 16). To obtain π_{ES}^{yy} and χ_{ES}^{yy}, we used Eqs. (22) and (23) along with HFSS numerical values for $T_{TM}(\theta)$ at 30° (the values for $|T_{TM}(30°)|$ are shown in Fig. 18). Although not shown here, π_{ES}^{yy} also has a resonance at 1.63 GHz, and χ_{ES}^{yy} also has a resonance at 2.33 GHz. Using these four retrieved surface parameters, along with Eq. (16), the transmission coefficient for various angles of incidence can be determined. The calculated values for $T_{TM}(\theta)$ from Eq. (16) for 30°, 45°, and 60° are shown in Fig. 18. For a comparison, we also show numerical results obtained from HFSS. This comparison shows that the transmission coefficients obtained from the retrieved surface parameters are indistinguishable from the HFSS results, even for angles as high as 60°. In fact, the "*Fano*" type resonances that occur around 2.4 GHz, 2.5 GHz, and 2.8 GHz are also captured using the retrieved surface parameters (Fig. 19 shows results zoomed in near these resonances). The differences in these very narrow Fano resonant frequencies do not exceed 0.05%.

4.6. Limit as the Surface-Area of the Apertures Diminishes

It is interesting to observe the surface parameters' behavior when the surface area of the apertures go to zero, or when the fill-factor (either l/p or a/p) approaches zero. Referring to the results in the various

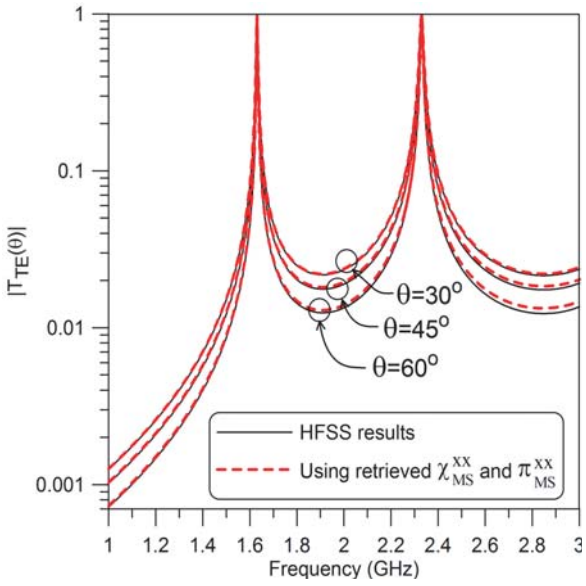

Figure 17. Comparison of $T_{TE}(\theta)$ for an array of square apertures filled with a high-contrast material ($\epsilon_r = 108.2$ and $\tan\delta = 4.9 \times 10^{-5}$) for $p = 26\,\text{mm}$, $h = 10\,\text{mm}$, and $l = 10\,\text{mm}$.

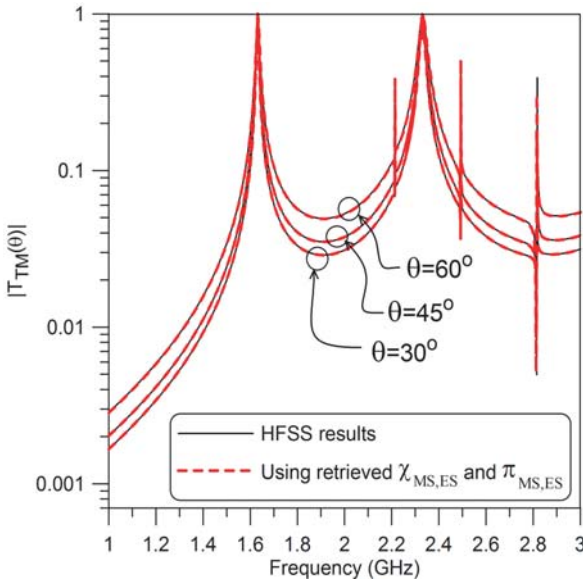

Figure 18. Comparison of $T_{TM}(\theta)$ for an array of square apertures filled with a high-contrast material ($\epsilon_r = 108.2$ and $\tan\delta = 4.9 \times 10^{-5}$) for $p = 26\,\text{mm}$, $h = 10\,\text{mm}$, and $l = 10\,\text{mm}$.

Figures, we see that as $l/p \to 0$ (or as $a/p \to 0$),

$$\begin{aligned} \pi_{ES}^{Ayy} &= \pi_{ES}^{Byy} \equiv 2\pi_{ES}^{yy} \to h/2 \\ \pi_{MS}^{Axx} &= \pi_{MS}^{Bxx} \equiv 2\pi_{MS}^{xx} \to -h/2, \\ \pi_{MS}^{Azz} &= \pi_{MS}^{Bzz} \equiv 2\pi_{MS}^{zz} \to -h/2 \end{aligned} \tag{24}$$

and

$$\begin{aligned} \chi_{ES}^{Ayy} &= \chi_{ES}^{Byy} \equiv \frac{1}{2}\chi_{ES}^{yy} \to h/2 \\ \chi_{MS}^{Axx} &= \chi_{MS}^{Bxx} \equiv \frac{1}{2}\chi_{MS}^{xx} \to -h/2. \\ \chi_{MS}^{Azz} &= \chi_{MS}^{Bzz} \equiv \frac{1}{2}\chi_{MS}^{zz} \to -h/2 \end{aligned} \tag{25}$$

These zero fill-factor limits are also obtained by observing how the surface parameters are defined in [11] (see Eqs. (73), (78) and (80) therein). The integrals involving the static field given in [11] are zero for $l/p = 0$ (or for $a/p = 0$), and hence the surface parameters reduce to $\pm h/2$. The physical reason for this is because of the choice of the reference plane location. This is made clear by looking at the reflection and transmission coefficients under the zero fill-factor condition. Using Eqs. (24) and (25) it can be shown that in this limit, Eqs. (11) and (12) reduce to:

$$R_{TE}(\theta) = -e^{-j\phi}; \quad T_{TE}(\theta) = 0 \tag{26}$$

where

$$\phi = \tan^{-1}\left(\frac{hk_0\cos\theta}{1 - \left(\frac{hk_0\cos\theta}{2}\right)^2}\right) \sim hk_0\cos\theta + O\left((hk_0)^3\right). \tag{27}$$

From Fig. 2 and [11], the reference plane is at $y = 0$ (i.e., half way between the top and bottom surfaces of the conducting plane). This reference plane represents the location where the GSTCs are applied. When no apertures are present in the plane, this would correspond to a phase shift of $hk_0\cos\theta$ for a

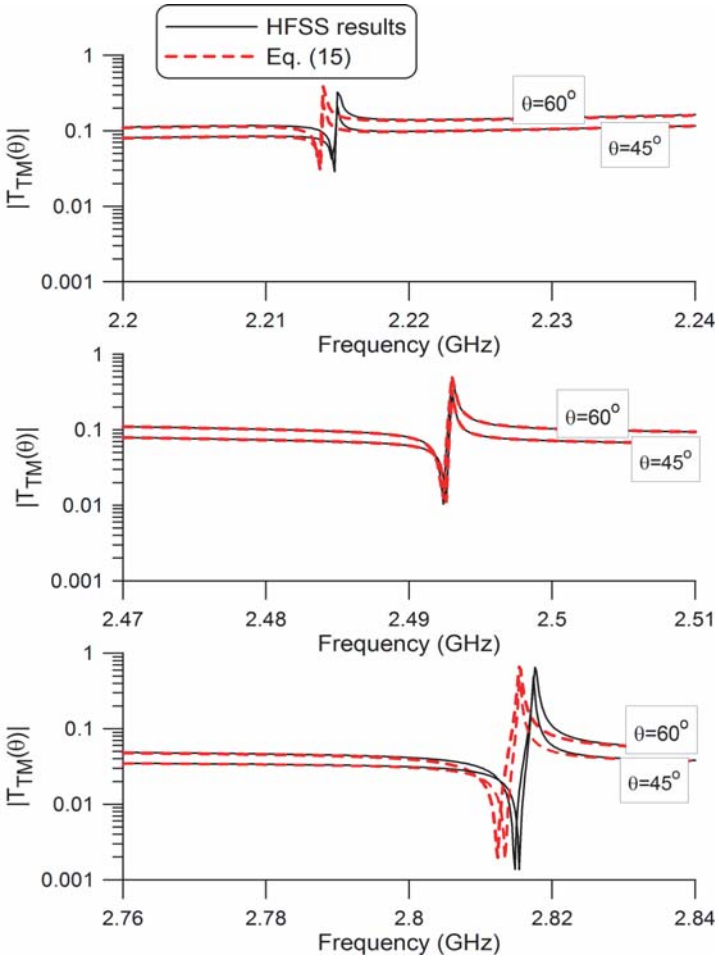

Figure 19. Zoomed-in region of *Fano* type resonances in $T_{TM}(\theta)$ at 45° and 60°.

reflected field relative to a position on the top side of the plane. This would correspond to the phase shift of a wave propagated from the top surface of the metascreen to $y = 0$ and back. If we had chosen a reference plane at some other location, the surface parameters for zero fill-factor would change accordingly. In any event, as $h \to 0$, this phase shift would also approach zero, and we would obtain the result for the reflection from a conducting plane as if a reference plane was on the surface (i.e., no phase shift).

4.7. Limit as the Apertures Touch

The other extreme limit of interest is when $l/p \to 1$ or $a/p \to 1/2$. For the square aperture, $l/p \to 1$ corresponds to the square apertures touching and as a result the screen disappearing (i.e., no conducting screen is present). From Figs. 10, and 11, we see that for this limit, χ_{ES} and χ_{MS} approach zero, and π_{ES} and π_{MS} approach ∞. This same behavior is observed for the metagrating analyzed in [12] (see Fig. 7 therein), where it is shown that as the radii of the wires composing the metagrating vanish, $\pi_{MS} \to \infty$ and $\chi_{(ES,MS)} \to 0$. Note that for circular apertures, the maximum possible fill-factor is $a/p = 1/2$. Although in this limit the circular apertures do touch, the conducting screen does not vanish. As a result, $\chi_{(ES,MS)}$ do not approach zero and and χ_{MS} and $\pi_{(ES,MS)}$ do not approach ∞. In the $a/p \to 1/2$ limit for circular apertures, all the surface parameters approach finite, non-zero, values.

5. DISCUSSION AND CONCLUSION

We have investigated the interaction of electromagnetic fields with a symmetric metascreen. The surface parameters (the effective electrical and magnetic surface susceptibilities and surface porosities) that appear explicitly in the GSTCs are uniquely defined, and as such serve as the physical quantities that most appropriately characterize the metascreen. The effective surface parameters for any given metascreen together with the GSTCs given in Eqs. (1) and (2) are all that are required to model its interaction with an EM field.

In this paper, we use the GSTCs to derive the reflection and transmission coefficients for a metascreen, which are expressed in terms of the electrical and magnetic surface parameters (surface susceptibilities and surface porosities). It is interesting to note that for TE-polarization, only two surface parameters (χ_{MS}^{xx} and π_{MS}^{xx}) are needed to fully characterize a metascreen which is in contrast to a metafilm, where three different surface parameters are needed to characterize a metafilm [1, 13, 14, 33]. On the other hand, for TM-polarization, four surface parameters (χ_{MS}^{zz}, π_{MS}^{zz}, χ_{ES}^{yy}, and π_{ES}^{yy}) are need to fully characterize a metascreen which is in contrast to a metafilm, where three different surface parameters are needed to characterize a metafilm for this polarization [1, 13, 14, 33].

We show that knowing the reflection and transmission coefficients (obtained either from measurements or numerical simulations) of a metascreen, we can develop retrieval techniques for determining the surface susceptibilities and surface porosities, and hence a method for uniquely characterizing the metascreen. We demonstrate this retrieval approach by showing results for metascreens composed of five different apertures (circular holes, square holes, crosses, and slots, and square apertures filled with a high-contrast dielectric). We show that internal resonances associated with the material filling the apertures can give rise to interesting reflection and transmission behavior, i.e., enhanced transmission when compared to apertures with no filling. We also discuss behavior of the surface parameters in the two extreme limits of the fill-factor.

We have considered only the case where the apertures and the array lattice have sufficient symmetry such that the magnetic surface susceptibilities and surface porosities of the resultant metascreen are diagonal (i.e., no cross-polarization terms). The presence of these more general GSTCs (cross-polarization or off-diagonal magnetic surface parameters) results in coupling between a TE and TM fields (i.e., a TE polarized field will generate TM fields and vice-versa), and the reflection and transmission coefficients for this more general case is the topic of a separate publication [32].

REFERENCES

1. Holloway, C. L., E. F. Kuester, J. A. Gordon, J. O'Hara, J. Booth, and D. R. Smith, "An overview of the theory and applications of metasurfaces: The two-dimensional equivalents of metamaterials," *IEEE Antennas and Propagation Magazine*, Vol. 54, No. 2, 10–35, April 2012.
2. Maradudin, A. A., *Structured Surfaces as Optical Metamaterials*, Cambridge University Press, Cambridge, UK, 2011.
3. Zouhdi, S., A. Sihvola, and M. Arsalane, *Advances in Electromagnetics of Complex Media and Metamaterials*, Kluwer Academic Pub., Boston, 2002.
4. Caloz, C. and T. Itoh, *Electromagnetic Metamaterials: Transmission Line Theory and Microwave Applications*, IEEE Press, Hoboken, NJ, 2005.
5. Eleftheriades, G. V. and K. G. Balmain, *Negative Refraction Metamaterials: Fundamental Principles and Applications*, IEEE Press, Hoboken, NJ, 2005.
6. Engheta, N. and R. W. Ziolkowski, *Electromagnetic Metamaterials: Physics and Engineering Explorations*, IEEE Press, Piscataway, NJ, 2006.
7. Marqués, R., F. Martín, and M. Sorolla, *Metamaterials with Negative Parameters: Theory, Design, and Microwave Applications*, Wiley-Interscience, Hoboken, NJ, 2008.
8. Capolino, F., *Metamaterials Handbook: Theory and Phenomena of Metamaterials*, CRC Press, Boca Raton, FL, 2009.
9. Cui, T. J., D. R. Smith, and R. Liu, *Metamaterials: Theory, Design, and Applications*, Springer, New York, 2010.

10. Kuester, E. F., M. A. Mohamed, M. Piket-May, and C. L. Holloway, "Averaged transition conditions for electromagnetic fields at a metafilm," *IEEE Trans. on Antennas and Propagation*, Vol. 51, No. 10, 2641–2651, 2003.
11. Holloway, C. L. and E. F. Kuester, "Generalized sheet transition conditions for a metascreen — A fishnet metasurface," *IEEE Trans. on Antennas and Propagation*, Vol. 66, No. 5, 2414–2427, 2018.
12. C. L. Holloway, E. F. Kuester, and A. Dienstfrey, "A homogenization technique for obtaining generalized sheet transition conditions for an arbitrarily shaped coated-wire grating," *Radio Science*, Vol. 49, No. 10, 813–850, 2014.
13. Holloway, C. L., A. Dienstfrey, E. F. Kuester, J. F. O'Hara, A. K. Azad, and A. J. Taylor, "A discussion on the interpretation and characterization of metafilms-metasurfaces: The two-dimensional equivalent of metamaterials," *Metamaterials*, Vol. 3, No. 2, 100–112, 2009.
14. Holloway, C. L., E. F. Kuester, and A. Dienstfrey, "Characterizing metasurfaces/metafilms: The connection between surface susceptibilities and effective material properties," *IEEE Ant. Wireless Prop. Lett.*, Vol. 10, 1507–1511, 2011.
15. Holloway, C. L. and E. F. Kuester, "A homogenization technique for obtaining generalized sheet transition conditions (GSTCs) for a metafilm embedded in a magneto-dielectric interface," *IEEE Trans. on Antennas and Propagation*, Vol. 64, No. 11, 4671–4686, 2016.
16. Kuester, E. F. and E. Liu, "Average transition conditions for electromagnetic fields at a metascreen of nonzero thickness," arXiv:1905.05871, arxiv.org, 2019.
17. Kuester, E. F., E. Liu, and N. J. Krull, "Average transition conditions for electromagnetic fields at a metascreen of vanishing thickness," arXiv:1905.05869, arxiv.org, 2019.
18. Nicolson, A. M. and G. Ross, "Measurement of the intrinsic properties of materials by time domain techniques," *IEEE Trans. Instrum. Meas.,* Vol. 19, No. 4, 377–382, 1970.
19. Weir, W. B., "Automatic measurements of complex dielectric constant and permeability at microwave frequencies," *Proc. IEEE*, Vol. 62, No. 1, 33–36, 1974.
20. Smith, D. R., S. Schultz, P. Markos, and C. M. Soukoulis, "Determination of effective permittivity and permeability of metamaterials from reflection and transmission coefficients," *Phys. Review B*, Vol. 65, 195104, 2002.
21. Ziolkowski, R. W., "Designs, fabrication, and testing of double negative metamaterials," *IEEE Trans. on Antennas and Propagation*, Vol. 51, No. 7, 1516–1529, 2003.
22. Kim, S., E. F. Kuester, C. L. Holloway, A. D. Scher, and J. Baker-Jarvis, "Boundary effects on the determination of the effective parameters of a metamaterials from normal incidence reflection and transmissions," *IEEE Trans. on Antennas and Propagation*, Vol. 59, No. 6, 2226–2240, 2011.
23. Kim, S., E. F. Kuester, C. L. Holloway, A. D. Scher, and J. R. Baker-Jarvis, "Effective material property extraction of a metamaterial by taking boundary effects into account at TE/TM polarized incidence," *Progress In Electromagnetics Research B*, Vol. 36, 1–33, 2012.
24. Chen, X., T. M. Grezegorczyk, B.-I. Wu, J. Pacheco, and J. A. Kong, "Robust method to retrieve the constitutive effective parameters of metamaterials," *Phys. Review E*, Vol. 70, 016608, 2004.
25. Weinstein, L. A., *The Theory of Diffraction and the Factorization Method*, The Golm Press, Boulder, CO, 1969.
26. Weinstein, L. A., "On the electrodynamic theory of grids," *Elektronika Bol'shikh Moshchnostei*, P. L. Kapitza and L. A. Weinstein, editors, Vol. 2, 26–74, Moscow, Nauka, 1963 [in Russian; Engl. transl. in *High-Power Electronics*, Vol. 2, Chapter II, 14–48, Pergamon Press, Oxford, 1966].
27. Senior, T. B. A. and J. L. Volakis, *Approximate Boundary Conditions in Electromagnetics*, 163, Institution of Electrical Engineers, London, 1995.
28. Sakurai, T., "Theory of electromagnetic wave on metallic mesh and grating," *J. Inst. Elec. Eng. Japan*, Vol. 68, 144–145, 1948 [in Japanese].
29. Kontorovich, M. I., "Averaged boundary conditions at the surface of a grating with a square mesh," *Radiotekh. Elektron.*, Vol. 8, 1506–1515, 1963 [in Russian; Engl. transl. in *Radio Eng. Electron. Phys.*, Vol. 8, 1446–1454, 1963].

30. Ricoy, M. A. and J. L. Volakis, "Derivation of generalized transition/boundary conditions for planar multiple-layer structures," *Radio Science*, Vol. 25, No. 4, 391–405, 1990.
31. Topsakal, E. and J. L. Volakis, "Surface integral equations for material layers modeled with tensor boundary conditions," *Radio Science*, Vol. 37, No. 4, 1053, 2002.
32. Holloway, C. L., E. F. Kuester, and A. H. Haddab, "Using reflection and transmission coefficients to retrieve surface parameters for an anisotropic metascreen: With a discussion on conversion between TE and TM polarizations," *Journal of Applied Phys.*, Vol. 125, 095102, 2019.
33. Holloway, C. L., M. A. Mohamed, and E. F. Kuester, "Reflection and transmission properties of a metafilm: With an application to a controllable surface composed of resonant particles," *IEEE Transactions on Electromagnetic Compatibility,* Vol. 47, No. 4, 853–865, 2005.
34. Holloway, C. L. and E. F. Kuester, "Equivalent boundary conditions for a perfectly conducting periodic surface with a cover layer," *Radio Science*, Vol. 35, No. 3, 661–681, 2000.
35. Auriault, J. L., "Effective macroscopic description for heat conduction in periodic composites," *Int. J. Heat Mass Transfer*, Vol. 26, 861–869, 1983.
36. Artola, M. and M. Cessenat, "Un problème raide avec homogénéisation en électromagnétisme," *Comptes Rendus Acad. Sci. Paris, sér. I*, Vol. 310, 9–14, 1990.
37. Holloway, C. L. and E. F. Kuester, "Impedance-type boundary conditions for a periodic interface between a dielectric and a highly conducting medium," *IEEE Trans. on Antennas and Propagation*, Vol. 48, No. 10, 1660–1672, 2000.
38. Chen, Y. and R. Lipton, "Resonance and double negative behavior in metamaterials," *Arch. Rat. Mech. Anal.*, Vol. 209, 835–868, 2013.
39. Bouchitté, G., C. Bourel, and D. Felbacq, "Homogenization near resonances and artificial magnetism in three dimensional dielectric metamaterials," *Arch. Rat. Mech. Anal.*, Vol. 225, 1233–1277, 2017.